

# Coupled Aqua and Ridge Planets in the Community Earth System Model

Xiaoning Wu<sup>1</sup>, Kevin A. Reed<sup>1</sup>, Christopher Lee Pitt Wolfe<sup>1</sup>, Gustavo Marques<sup>2</sup>, Scott Daniel Bachman<sup>2</sup>, and Frank O. Bryan<sup>3</sup>

<sup>1</sup>Stony Brook University

<sup>2</sup>NCAR

<sup>3</sup>National Center for Atmospheric Research (UCAR)

November 30, 2022

## Abstract

Idealized models can reveal insights into Earth's climate system by reducing its complexities. However, their potential is undermined by the scarcity of fully coupled idealized models with components comparable to contemporary, comprehensive Earth System Models. To fill this gap, we compare and contrast the climates of two idealized planets which build on the Simpler Models initiative of the Community Earth System Model (CESM). Using the fully coupled CESM, the Aqua configuration is ocean-covered except for two polar land caps, and the Ridge configuration has an additional pole-to-pole grid-cell-wide continent. Contrary to most sea surface temperature profiles assumed for atmosphere-only aquaplanet experiments with the thermal maximum on the equator, the coupled Aqua configuration is characterized by a global cold belt of wind-driven equatorial upwelling, analogous to the eastern Pacific cold tongue. The presence of the meridional boundary on Ridge introduces zonal asymmetry in thermal and circulation features, similar to the contrast between western and eastern Pacific. This zonal asymmetry leads to a distinct climate state from Aqua, cooled by  $\sim 2^{\circ}\text{C}$  via the radiative feedback of clouds and water vapor. The meridional boundary of Ridge is also crucial for producing a more Earth-like climate state compared to Aqua, including features of atmospheric and ocean circulation, the seasonal cycle of the Intertropical Convergence Zone, and the meridional heat transport. The mean climates of these two basic configurations provide a baseline for exploring other idealized ocean geometries, and their application for investigating various features and scale interactions in the coupled climate system.

# Coupled Aqua and Ridge Planets in the Community Earth System Model

Xiaoning Wu<sup>1</sup>, Kevin A. Reed<sup>1</sup>, Christopher L. P. Wolfe<sup>1</sup>, Gustavo M. Marques<sup>2</sup>, Scott D. Bachman<sup>2</sup>, Frank O. Bryan<sup>2</sup>

<sup>1</sup>School of Marine and Atmospheric Sciences, Stony Brook University, Stony Brook, NY

<sup>2</sup>Climate and Global Dynamics Laboratory, National Center for Atmospheric Research, Boulder, CO

## Key Points:

- Two baseline examples of fully coupled CESM with idealized ocean geometry, Aqua and Ridge, are presented
- With sufficient resolution, coupled Aqua has a global cold belt of equatorial upwelling and corresponding “reverse Hadley” cells
- Ridge’s zonal asymmetry is crucial for making its circulations more Earth-like compared to Aqua

---

Corresponding author: Xiaoning Wu, [xiaoning.wu.1@stonybrook.edu](mailto:xiaoning.wu.1@stonybrook.edu)

## Abstract

Idealized models can reveal insights into Earth’s climate system by reducing its complexities. However, their potential is undermined by the scarcity of fully coupled idealized models with components comparable to contemporary, comprehensive Earth System Models. To fill this gap, we compare and contrast the climates of two idealized planets which build on the Simpler Models initiative of the Community Earth System Model (CESM). Using the fully coupled CESM, the Aqua configuration is ocean-covered except for two polar land caps, and the Ridge configuration has an additional pole-to-pole grid-cell-wide continent. Contrary to most sea surface temperature profiles assumed for atmosphere-only aquaplanet experiments with the thermal maximum on the equator, the coupled Aqua configuration is characterized by a global cold belt of wind-driven equatorial upwelling, analogous to the eastern Pacific cold tongue. The presence of the meridional boundary on Ridge introduces zonal asymmetry in thermal and circulation features, similar to the contrast between western and eastern Pacific. This zonal asymmetry leads to a distinct climate state from Aqua, cooled by  $\sim 2^{\circ}\text{C}$  via the radiative feedback of clouds and water vapor. The meridional boundary of Ridge is also crucial for producing a more Earth-like climate state compared to Aqua, including features of atmospheric and ocean circulation, the seasonal cycle of the Intertropical Convergence Zone, and the meridional heat transport. The mean climates of these two basic configurations provide a baseline for exploring other idealized ocean geometries, and their application for investigating various features and scale interactions in the coupled climate system.

## Plain Language Summary

Simplified climate models can improve our understanding of the Earth’s climate system by stripping down its complexities. Previous simplified climate models — with idealized ocean shapes — have laid great groundwork, but their coarse resolution and overly reduced model components are hard to relate to contemporary models for international climate assessments. We fill this gap by presenting two simplified climate models with components and resolution similar to that of state-of-the-art Earth system models. Aqua is ocean-covered except for two polar land caps, and Ridge has an additional pole-to-pole strip continent. Ridge’s ocean, like the Pacific, has a western pool and eastern cold tongue upwelled from below. On Aqua, without continents blocking the east-west direction, the equatorial upwelling extends globally, forming a cold belt. This results in a warmer global climate on Aqua than Ridge, as clouds over Ridge’s warm pool reflect away more solar radiation than Aqua’s cold and dry equatorial region. Ridge’s strip continent in the north-south direction makes its climate more Earth-like than Aqua, including circulation and poleward transport of energy. The capacity of the Aqua and Ridge planets enables the application to problems of scientific interest and societal impacts, such as El Niño and hurricanes.

## 1 Introduction

Idealized models are illuminating tools for understanding Earth’s climate system (Held, 2005; Maher et al., 2019). By reducing the complexities of the coupled climate system in terms of boundary conditions or model physics, idealized models have helped advance the scientific understanding of various aspects and scales of the climate system (e.g., Manabe & Bryan, 1969; Ferreira et al., 2010; Wolfe & Cessi, 2010; Abernathey et al., 2013; Voigt & Shaw, 2015; Chavas et al., 2017; Brunetti et al., 2019), as well as the evaluation and development of climate model components (Chang et al., 2001; Reed & Jablonowski, 2012; Bachman & Fox-Kemper, 2013; Herrington & Reed, 2017). The availability of idealized models, embedded within a hierarchy of complexity leading up to state-of-the-art, comprehensive Earth System Models used for climate projection and assess-

ments (Eyring et al., 2016), can serve as a valuable resource for climate research and education (Jeevanjee et al., 2017; Polvani et al., 2017; Schultz et al., 2017).

Focusing on the atmosphere-ocean system, ocean-covered representations of Earth (commonly referred to as aquaplanets) have been widely used for either the atmospheric or ocean component at various degree of complexity, but fully coupled configurations are relatively scarce. For the atmospheric component, there is a rich history of application for aquaplanets (Neale & Hoskins, 2000; Blackburn et al., 2013), with either prescribed sea surface temperature (e.g., Medeiros et al., 2016) or slab ocean configurations (e.g., Donohoe et al., 2014; Benedict et al., 2017) as the simplified lower boundary condition, forgoing ocean dynamics. Example topics of study using aquaplanet configurations include the hemispheric asymmetry in tropical rainfall (Frierson et al., 2013), the length scale of extratropical storm tracks (Kaspi & Schneider, 2011), and the effect of off-equatorial thermal forcing on tropical cyclone activity (Ballinger et al., 2015). For the ocean component forced by a prescribed atmosphere, idealized ocean basins are used for understanding the overturning circulation (Wolfe & Cessi, 2010; Jones & Cessi, 2016; Cessi & Jones, 2017; Ferrari et al., 2017) and factors affecting salinity (Jones & Cessi, 2017, 2018). For global and coupled configurations, earlier works (Smith et al., 2006; Farneti & Vallis, 2009) have explored the global climates of selected ocean geometries. Other notable examples using coupled aquaplanets include a hierarchy of idealized ocean geometries (Marshall et al., 2007; Enderton & Marshall, 2009; Ferreira et al., 2010). These simplified designs demonstrate remarkable resemblance to the observed Earth climate on the planetary scale, including the meridional heat transport (Czaja & Marshall, 2006; Marshall et al., 2007; Enderton & Marshall, 2009) and ocean salinity contrast (Ferreira et al., 2010; Nilsson et al., 2013). However, these configurations, oriented towards the global-scale ocean circulation with extremely simplified atmospheres (e.g., Molteni, 2003) at  $\sim 3^\circ$  horizontal resolution or coarser, do not aim to address important atmospheric processes that depend on higher horizontal and vertical resolution, or more complete model physics (Ballinger et al., 2015; Herrington & Reed, 2017).

In summary, a gap is present in the hierarchy between previously available idealized models and comprehensive Earth System Models. Specifically, there is currently no coupled idealized model available with comprehensive model physics equivalent to those used for the Coupled Model Intercomparison Project (CMIP; Eyring et al., 2016) for both the atmospheric and ocean components. This lack of availability undermines the application of idealized modeling to process-level understanding of CMIP-class models where atmosphere-ocean coupling plays a key role, and precludes the full investigation of scale interactions of scientific and societal interest at the atmosphere-ocean interface (e.g., Scoccimarro et al., 2017; Carranza et al., 2018; Li & Sriv, 2018).

To fill this gap, by building on the Simpler Models initiative (Polvani et al., 2017, <http://www.cesm.ucar.edu/models/simpler-models>) of the Community Earth System Model (CESM; Hurrell et al., 2013; Danabasoglu et al., 2020), we have developed two fully coupled baseline configurations with idealized ocean geometry. The new development brings unique, CMIP-relevant modeling capabilities into the idealized framework. In this study, we present the mean climates of the two configurations and discuss the contrast between them. The first one, Aqua, is ocean-covered except for minimal polar land caps; the second one, Ridge, has a single meridional boundary. Comparing and contrasting with previous idealized studies, these two configurations demonstrate the role of ocean geometry in the coupled climate state, including impacts on meridional heat transport. The assessment of these two basic configurations provides a baseline for exploring additional forms of idealized ocean geometries, and their application to the study of various features and scale interactions in the coupled climate system.

This paper is organized as follows. Section 2 describes the details of model configuration, and the simulation data under analysis. Section 3 presents the mean climates of the CESM Aqua and Ridge planets from the perspectives of the energy budget, the

large-scale circulation, and the meridional heat transport. Finally, Section 4 discusses the results in the context of previously documented models, and the outlooks for future work.

## 2 Data and Methods

The idealized configurations are developed in the framework of CESM (Hurrell et al., 2013; Danabasoglu et al., 2020), a state-of-the-art, community modeling tool. With numerous options for configuration and a vibrant user community, CESM provides the capacity to produce simulations for international climate assessments (Eyring et al., 2016), as well as reduced-complexity options for fundamental investigations and continued model component development (Polvani et al., 2017). We expand on currently available options of atmosphere-only or slab ocean aquaplanets (Medeiros et al., 2016; Benedict et al., 2017), and introduce fully coupled configurations with dynamical ocean.

Two types of idealized ocean geometries are configured, as shown in Fig. 1. For Aqua, the planet is ocean-covered except for two polar continents that reach down to 80°N/S. The presence of the polar continents, occupying minimal area, is required by the ocean grid. For Ridge (Smith et al., 2006; Enderton & Marshall, 2009), a single grid-cell-wide strip of pole-to-pole continent is added as a meridional boundary for the ocean basin. All land has zero orography.

The atmospheric component is the Community Atmosphere Model version 4 (CAM4; Neale et al., 2010). The choice of model version is made to balance complexity and computational cost. The finite-volume dynamical core, based on a regular latitude-longitude grid, is built upon a 2D shallow water approach (Lin & Rood, 1996, 1997) and mass-conservative in flux-form. The parameterization schemes include deep convection (Zhang & McFarlane, 1995), shallow moist convection (Hack, 1994), dry boundary layer turbulence (Holtslag & Boville, 1993), and cloud physics, radiation, etc. further described in Neale et al. (2010). The horizontal resolution is nominally 1°, resulting in grid spacing of ~110 km in the tropical regions. In the vertical direction, the model is divided into 26 layers in a hybrid sigma-pressure coordinate system, with finer spacing near model bottom and top (~3 hPa). Settings for the solar constant, dry mass, greenhouse gas concentrations, ozone distribution, and aerosols are adapted from the Aqua-Planet Experiment (Neale & Hoskins, 2000).

The ocean component is the Modular Ocean Model version 6 (MOM6; Adcroft et al., 2019), the latest update to replace the previous CESM ocean component starting with CESM3. One advantage of MOM6 is the versatile specification of vertical layers via the use of the Arbitrary-Lagrangian-Eulerian algorithm (Hirt et al., 1974; Bleck, 1978). The horizontal resolution is nominally 2°, with equatorial refinement to 1°. The ocean maximum depth is 4000 m, divided into 57 vertical layers, with thickness decreasing from ~250 m at the bottom to 2.5 m near the ocean surface. The effects of mesoscale eddies are parameterized by activating two schemes in the tracer equation. The first scheme follows the ideas of Gent et al. (1995), where available potential energy is removed from the large scale by flattening isopycnals. A constant thickness diffusivity of  $2000 \text{ m}^2 \text{ s}^{-1}$  is used without any vertical structure. The associated eddy-induced transport is applied as a bolus velocity. To avoid the problems associated with layer thickness diffusion described by Holloway (1997), this scheme is implemented as an interface height diffusion. Following Solomon (1971) and Redi (1982), the second scheme represents the diffusive mixing of tracers along neutral surfaces, which is implemented using a finite-volume general-coordinate methodology. Again, a constant along-isopycnal tracer diffusivity of  $2000 \text{ m}^2 \text{ s}^{-1}$  is used. The K-Profile vertical mixing Parameterization (KPP; Large et al., 1994) is applied via the Community ocean Vertical Mixing (CVMix; Griffies et al., 2015) framework. The diapycnal diffusivity is  $2 \times 10^{-5} \text{ m}^2 \text{ s}^{-1}$ , the Laplacian horizontal viscosity is  $1 \times 10^4 \text{ m}^2 \text{ s}^{-1}$ , and the coefficient for quadratic bottom drag is 0.005. To provide to-

pographic form drag for balancing the momentum input from the atmosphere, we prescribe zonally and hemispherically symmetric bottom topography in analytical, sinusoidal form (see Fig. S1). This is particularly important for the Aqua case, and we use the same bottom topography in both cases for consistency. The bottom topography has the maximum height of 500 m in the vertical, with horizontal length scale of 1000 km in the meridional direction, and  $45^\circ$  in the zonal direction. These length scales are chosen to avoid subgrid-scale signals.

The sea ice component is the Community Ice CodE version 5 (CICE5; Bailey et al., 2018), with full thermodynamics and dynamics. Since the quasi-equilibrium climate states of both configurations are too warm for sea ice formation (see Table 1), the sea ice component is present but not active for the period under analysis in the present study. As needed by the minimal presence of land, the land component is the Community Land Model version 5 (CLM5; Lawrence et al., 2019) at the same horizontal resolution as the atmospheric component. For the polar and ridge continents, the land surface type is set to wetland, which behaves most similarly to a slab ocean in comparison with other land surface types. Precipitation over land, a small amount, is returned to the ocean by adjusting the water balance in the MOM6 component. The coupling is handled by the Common Infrastructure for Modeling the Earth (CIME; <http://github.com/ESMCI/cime>, see description in Danabasoglu et al. (2020)). The coupling frequency for all components is hourly, based on the spatial resolution of model components.

For both Aqua and Ridge configurations, the diurnal cycle is retained, and an idealized seasonal cycle is imposed by setting the orbital obliquity to  $23.3^\circ$ . Model initialization is zonally symmetric for all components (atmosphere, ocean, land, and sea ice). On the National Science Foundation (NSF)-supported Cheyenne supercomputer housed at the National Center for Atmospheric Research (NCAR), the model achieves throughput of  $\sim 80$  simulated years per wall-clock day, while archiving annually averaged output for the ocean and monthly averaged output for all other components. By Year 400 of the 500-year integration, although the deep ocean is still drifting, the top-of-atmosphere (TOA) radiative balance has adjusted close to equilibrium for both configurations (imbalance  $\sim O(0.1) \text{ Wm}^{-2}$ , see Table 1 and Fig. S2). We discuss the climate state of Year 401–500 in the following section, using monthly averaged output for the atmosphere and annually averaged output for the ocean.

### 3 Results

Fig. 1 illustrates the state of the coupled Aqua and Ridge planets, with snapshots of their oceans and atmospheres in boreal summer. Both planets are warm and ice-free. For the zonally symmetric Aqua, the sea surface temperature (SST; Fig. 1a) shows a global cold belt of equatorial upwelling that persists through the seasonal cycle (see animation in supplement). A common feature of coupled Aqua configurations with dynamical oceans (Smith et al., 2006; Marshall et al., 2007; Farneti & Vallis, 2009), this local SST minimum on the equator is markedly different from the typical SST patterns used for atmosphere-only Aqua-Planet Experiments (Neale & Hoskins, 2000). For Ridge (Fig. 1b), the presence of the meridional boundary leads to the formation of a western warm pool, limiting the global equatorial upwelling of Aqua to eastern upwelling in the cold tongue. Analogous to the Pacific, besides the local equatorial upwelling, the equatorward eastern boundary current also contributes to the cold tongue via advection (Wyrski, 1981; Kessler, 2006). These SST patterns, in turn, influence the characteristics of their atmospheres. Both planets exhibit a rich variety of synoptic systems, including extratropical storms and tropical cyclone-like vortices (Fig. 1c–d). For Aqua (Fig. 1c), on either side of the cold and dry equator, the atmosphere is remarkably rich in moisture even in the winter hemisphere. This is associated with Aqua’s unique circulation patterns in the seasonal cycle, discussed later in Section 3.2. For Ridge (Fig. 1d), the winter hemisphere is noticeably drier compared to its summer hemisphere, especially around the cold tongue and the eastern bound-

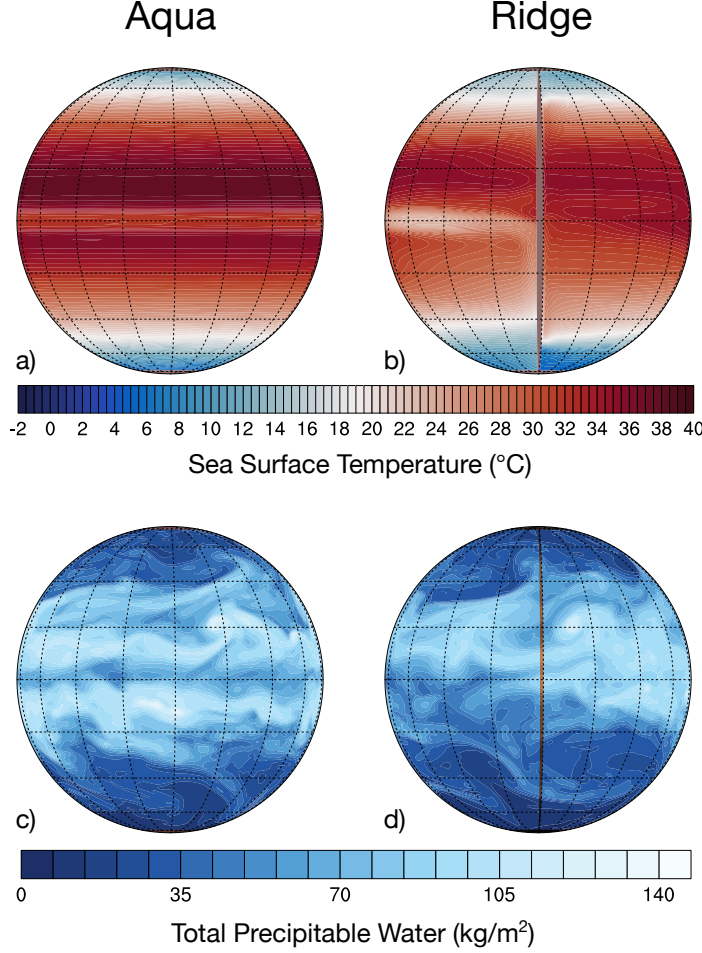


**Figure 1.** Illustration of the Aqua and Ridge planets. The polar land caps and the ridge continent are marked in brown. (a–b) SST ( $^{\circ}\text{C}$ ) for August (100-yr climatology), showing the global cold belt of equatorial upwelling on Aqua, and the eastern and western boundary currents on Ridge (see animation of the seasonal cycle in supplement); (c–d) Instantaneous snapshots of total precipitable water ( $\text{kgm}^{-2}$ ) from boreal summer, displaying various synoptic systems.

any current. The presence of the western warm pool is reflected in the rich reservoir of atmospheric moisture in the region.

The contrast in these thermodynamic and dynamic features, with an emphasis on the zonal asymmetry of Ridge, is further detailed in Fig. 2 with the 100-year climatology. For Aqua (Fig. 2, left column), the equatorial atmosphere is uniformly associated with subsidence (Fig. 2a), as a result of local SST minimum in the equatorial region. Driven by mild easterly wind stress (Fig. 2c), the equatorial belt of upwelling (Fig. 2e) produces a shallow thermocline in the ocean underneath (Fig. 2i). In contrast, Ridge (Fig. 2, right column) produces many Pacific-like features: a Walker-like circulation (Fig. 2b) develops, with convection over the moist western warm pool, and subsidence over the dry eastern cold tongue; the convergence of zonal wind stress around  $120^{\circ}\text{E}$  (Fig. 2d) marks the location of the warmest equatorial SST (Fig. 2f), producing a zonal SST gradient of  $\sim 8^{\circ}\text{C}$  averaged over  $5^{\circ}\text{N}$ – $5^{\circ}\text{S}$  (Fig. 2h), contrary to Aqua’s zonal uniformity (Fig. 2g). Corre-



**Table 1.** Statistics of the global mean, annually averaged over Year 401-500. Global mean ocean salinity is a constant value of 34.969 psu for both planets, due to the absence of sea ice.

	Unit	Aqua		Ridge	
		Avg.	Stdev.	Avg.	Stdev.
Surface temperature	°C	27.466	0.104	25.503	0.071
Surface pressure	hPa	1016.580	0.067	1015.690	0.040
Total cloud fraction	fraction	0.444	0.002	0.472	0.004
Cloud radiative forcing	Wm <sup>-2</sup>	-23.166	0.250	-25.857	0.315
Total precipitable water	kgm <sup>-2</sup>	58.070	0.694	49.194	0.396
Precipitation rate	mmday <sup>-1</sup>	4.384	0.020	4.182	0.014
Net shortwave (TOA)	Wm <sup>-2</sup>	261.507	0.223	257.822	0.345
Net longwave (TOA)	Wm <sup>-2</sup>	261.129	0.286	258.091	0.236
Net shortwave (ocean surface)	Wm <sup>-2</sup>	183.856	0.318	181.852	0.390
Net longwave (ocean surface)	Wm <sup>-2</sup>	-44.443	0.378	-48.341	0.252
Downwelling longwave (ocean surface)	Wm <sup>-2</sup>	424.391	1.057	408.145	0.644
Latent (ocean surface)	Wm <sup>-2</sup>	-129.284	0.586	-123.159	0.387
Sensible (ocean surface)	Wm <sup>-2</sup>	-9.683	0.107	-10.578	0.092
Ocean potential temperature	°C	8.566	0.015	7.553	0.026

spondingly, the equatorial thermocline (Fig. 2j) deepens from the eastern end: the 18°C isotherm deepens all the way to ~300 m at the western boundary, whereas the 28°C isotherm reaches maximum depth in the middle of the ocean basin before shoaling again in the west. Note that with active atmosphere, the western warm pool is established at a distance away from the western boundary (~ 1/3 of the basin width), as opposed to immediately against the western boundary in an ocean-only model forced by prescribed, zonally uniform wind.

The fundamental role of the meridional ocean boundary in determining the global climate, as suggested by Figs. 1 and 2, are further analyzed in the subsections below. Contrasting the climates of Aqua and Ridge, we explore the following aspects: the global energy budget, the large-scale circulation with seasonality, and the resulting meridional heat transport.

### 3.1 Global Energy Budget and Balance

The differences between the global mean climates of Aqua and Ridge is presented in Table 1, which summarizes the statistics of global mean values concerning the energy budget and the water cycle over the annually averaged 100-year period under analysis. In virtually all aspects, the differences between the global mean state of Aqua and Ridge are well beyond the range of their respective interannual variability, as measured by the standard deviation of the global mean.

The warmth of the climate states — with ~27°C global mean surface temperature for Aqua — are comparable to Smith et al. (2006), although greater contrast between Aqua and Ridge is presented here. Aqua is ~2°C warmer in global mean surface temperature and ~1°C warmer in global mean ocean potential temperature compared to Ridge (Table 1). In the energy budget, this corresponds to greater net shortwave heating at TOA, as well as at the ocean surface. The radiative forcing of clouds plays a large role in the cooling of Ridge relative to Aqua: the prominent cloud radiative cooling in the tropics, due to the presence of the western warm pool on Ridge with its convective activities, is reflected in the global mean.



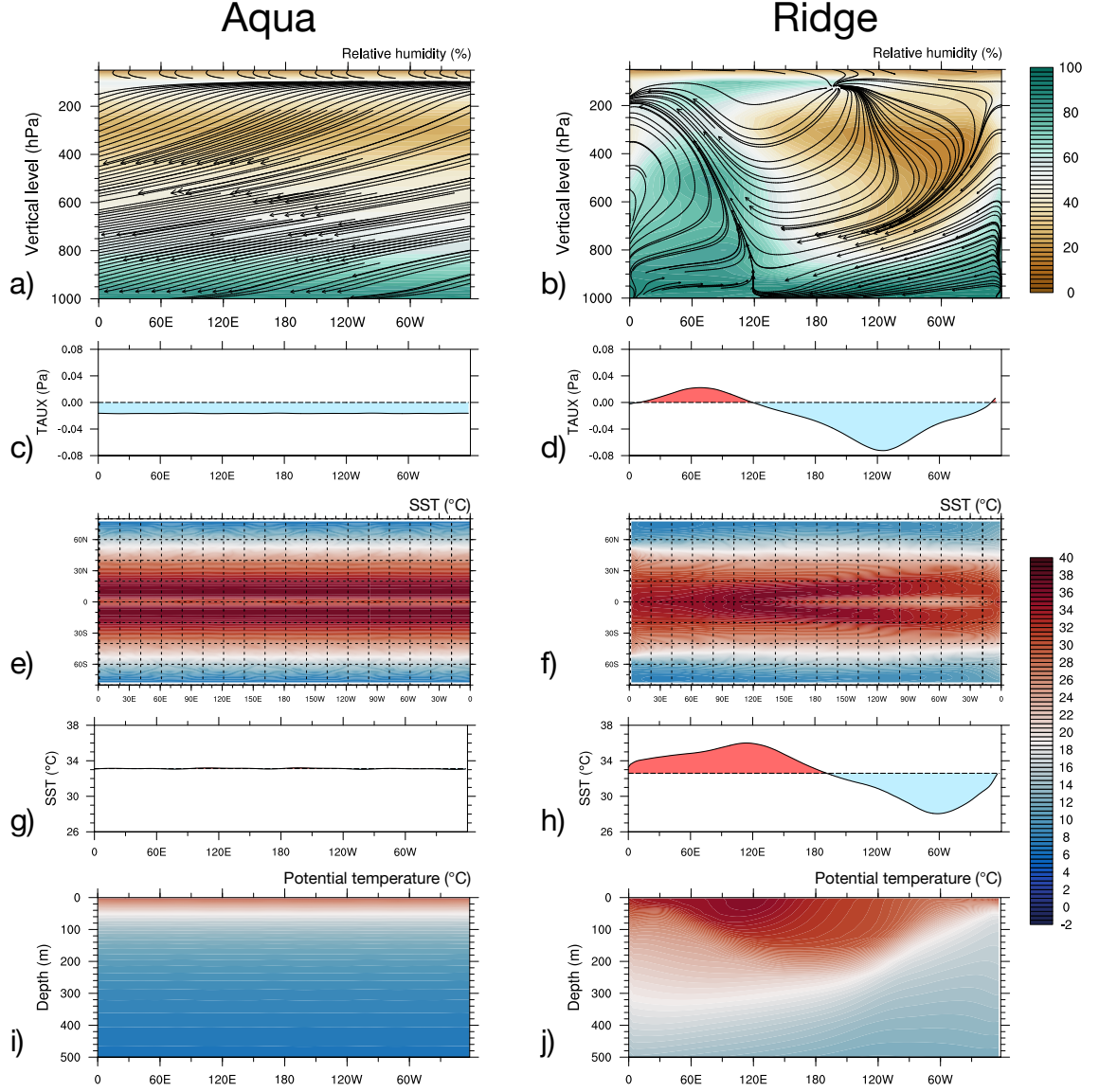


**Figure 2.** Zonal features in the tropics, 100-yr climatology: (a–b) Zonal circulation in the atmosphere with Walker-like feature on Ridge, seen in relative humidity (colored shading), and streamline of zonal and vertical velocity (solid arrows). Vertical velocity is scaled by a factor of 50 for visualization; (c–d) Zonal gradient of zonal wind stress (Pa), the dashed horizontal line marking zero; (e–f) SST (°C); (g–h) Zonal gradient of SST (°C), the dashed horizontal line marking the zonal average value; (i–j) Equatorial thermocline, as seen in potential temperature (°C). All panels except for (e–f) are averaged 5°N–5°S.

The meridional structure of the energy budget is further detailed in Fig. 3. In the zonal average of the TOA radiative budget (Fig. 3a–d), both Aqua and Ridge qualitatively resemble Earth observations (e.g., Stephens et al., 2015). The extent of the tropics is essentially identical for both planets, with poleward limits at 37.2°N/S as defined by TOA radiative surplus. In the zonal average, the net tropical heating of Aqua is greater relative to Ridge at both TOA and the ocean surface. At TOA, Aqua receives more shortwave (Fig. 3a–b) and integrated net surplus heating (Fig. 3c–d) than Ridge. Over the ocean surface (Fig. 3e–f), the heating of Aqua relative to Ridge in the deep tropics is mostly due to greater net shortwave and lesser latent heat loss over the equatorial cold belt (see Fig. S3). Specifically, the presence of the western warm pool on Ridge (Fig. 2, right column) reduces surface shortwave flux via cloud forcing, and enhances latent heat loss of the ocean by greater evaporation associated with its warmer temperature. These effects are analogous to observed surface heat fluxes in the Pacific (e.g., Grist & Josey, 2003), where the Eastern Pacific cold tongue is a region of greater ocean heating than the rest of tropical Pacific. In this sense, these heating effects are expanded to the entire equatorial cold belt on Aqua, contributing to its warmer climate.

The warmer climate of Aqua reinforces a more intense water cycle than Ridge. In the global average (Table 1), Aqua’s intensified water cycle relative to Ridge is reflected in its slightly higher surface pressure due to water vapor pressure, higher total precipitable water by 18%, and higher precipitation rate by 4.8% (Table 1). The percentage of precipitation increase on Aqua relative to Ridge is consistent with the latent heating of their atmospheres, at a lesser fractional increase than for total precipitable water, as discussed by Pendergrass and Hartmann (2014). Aqua’s fractional increase of precipitation with regard to global mean surface temperature is also in line with those reported from CMIP5 warming experiments (Collins et al., 2013). On Aqua, the higher amount of water vapor – a greenhouse gas – helps to maintain its warm state, as shown in the dramatic warming by downwelling longwave compared to Ridge (Table 1). Furthermore, the meridional structures of some relevant fields are shown in Fig. 4, and the zonally averaged vertical structures of moisture and salinity are shown in Fig. 5. In the zonal average, both planets have two Intertropical Convergence Zones (ITCZs), with Aqua having higher peaks in precipitation (Fig. 4b) and moisture (Fig. 5a–b) than Ridge. The resulting patterns of freshwater forcing (Fig. 4h) correspond to near-surface salinity of the ocean (Fig. 5c–d). It is worth noting that “double ITCZs” are a common feature of atmosphere-only aquaplanets with prescribed equatorial thermal maximum (Blackburn et al., 2013; Medeiros et al., 2016), and the coupled SST patterns of Aqua and Ridge (Fig. 4a) are perhaps even more conducive to such structures.

As defined by the TOA radiative budget in Fig. 3, the boundary of the tropics and the descending branch of the Hadley cell (see Fig. 8a–b and later discussion) coincides with many dynamical features in the zonal average (Fig. 4): the peaks in surface pressure (Fig. 4c), the switching of direction of zonal wind stress (Fig. 4e) and peaks in wind stress curl (Fig. 4f), and the deepening of the mixed layer depth towards higher latitudes (Fig. 4g). In Fig. 4g, the zonal asymmetry in Ridge’s tropical thermocline (Fig. 2) is responsible for deeper mixed layer depth in the deep tropics than Aqua. These contrasts in the circulation pattern are further discussed in the next subsection.

### 3.2 Large-Scale Circulation

For both the atmosphere and the ocean, Fig. 6 shows features of the horizontal circulation, while Fig. 7 shows the vertical structures of the zonally averaged zonal flows.

For the atmosphere, the impact of ocean geometry is mediated by SST. In the surface pressure field (Fig. 6a–b), compared to Aqua’s zonally uniform belt of subtropical high, Ridge has more defined centers of subtropical highs over its eastern boundary currents (see Fig. 6b). In the vertical structure, the contrast between the zonally averaged

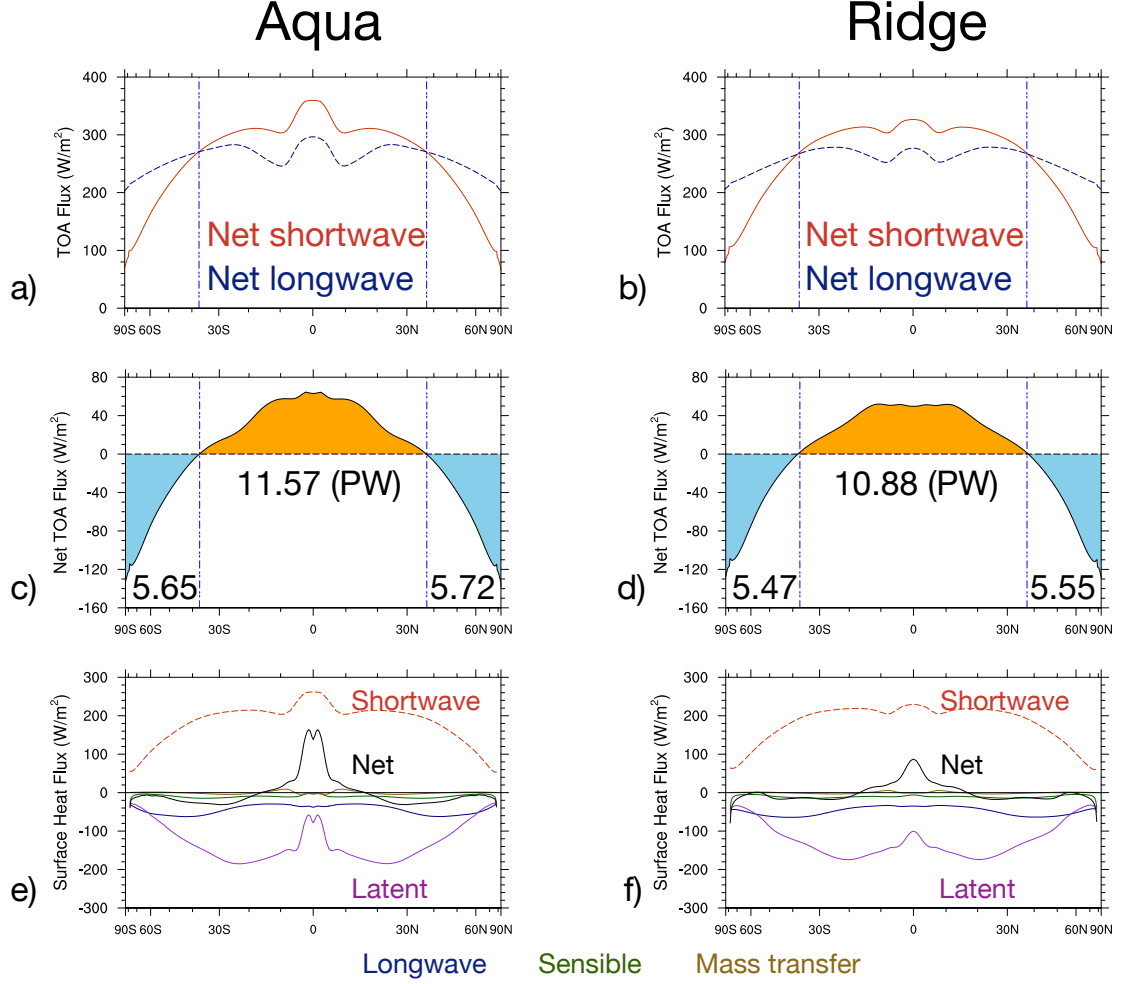


**Figure 3.** Zonally averaged energy budgets, 100-yr climatology: (a-b) Top-of-atmosphere (TOA) fluxes ( $\text{Wm}^{-2}$ ); (c-d) Net TOA flux ( $\text{Wm}^{-2}$ ) derived from (a-b), labeled with the integrated total amount of tropical surplus (shaded in orange) and extratropical deficit (shaded in blue), in petawatt (PW); (e-f) Ocean surface heat fluxes ( $\text{Wm}^{-2}$ ). The x-axis is scaled by  $\sin(\text{lat})$  to reflect the proportion of surface area, with minor tick marks at  $10^\circ$  intervals.

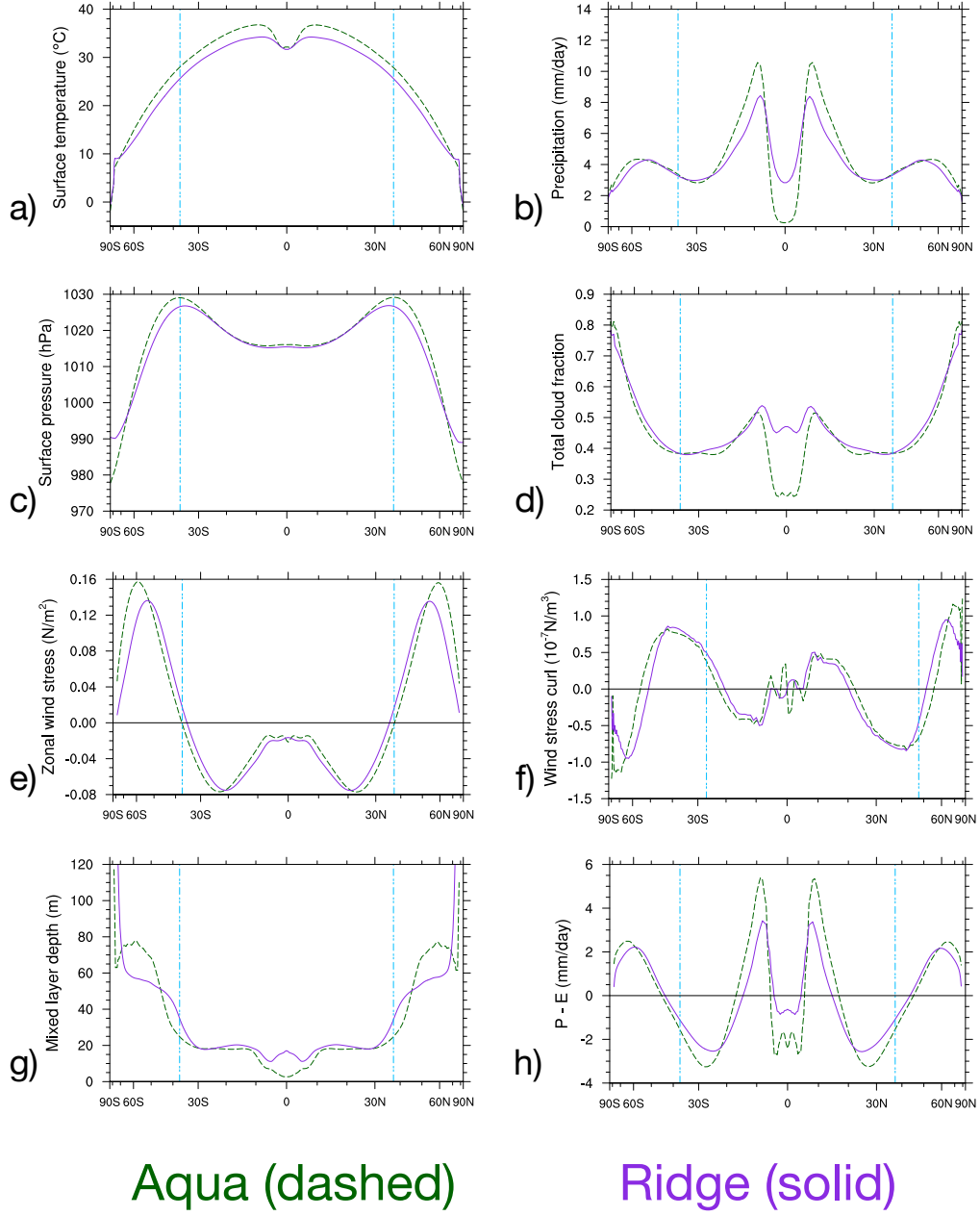


**Figure 4.** Zonal average profiles, 100-yr climatology: (a) Surface temperature ( $^{\circ}\text{C}$ ); (b) Precipitation rate ( $\text{mmday}^{-1}$ ); (c) Surface pressure (hPa); (d) Total cloud fraction (fraction); (e) Zonal wind stress ( $\text{Nm}^{-2}$ ); (f) Curl of zonal wind stress ( $10^{-7} \text{Nm}^{-3}$ ); (g) Ocean mixed layer depth (m); (h) Precipitation minus evaporation ( $\text{mmday}^{-1}$ ). The vertical blue lines mark the extent of the tropics, as defined by TOA radiative budget (see Fig. 3).

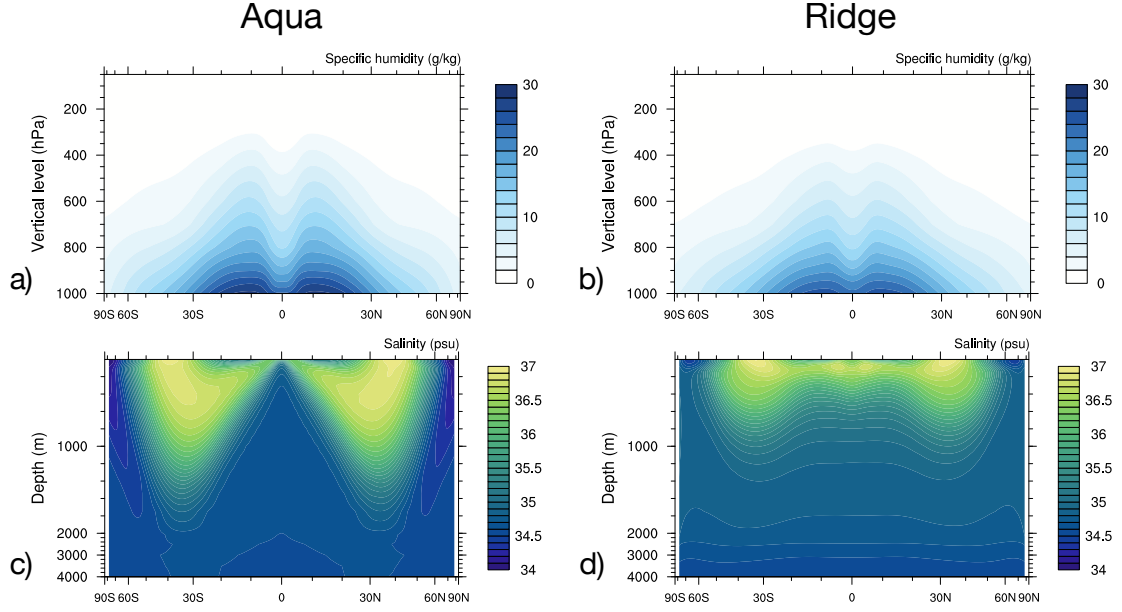


**Figure 5.** Zonally averaged vertical sections, 100-yr climatology: (a–b) Specific humidity ( $\text{gkg}^{-1}$ ); (c–d) Salinity (psu). For the ocean (c–d), the depths below 2000 m are linearly shrunk as labeled.

zonal wind of Aqua and Ridge (Fig. 7a–b) is influenced by their surface temperature gradients (Fig. 4a) through the thermal wind relationship (cf. Enderton & Marshall, 2009). Due to enhanced ocean heat transport to the extratropics via western boundary currents (cf. Enderton & Marshall, 2009; Vallis & Farneti, 2009), the meridional gradient of Ridge’s surface temperature is flattened relative to Aqua (Fig. 4a). Consequently, the greater surface temperature gradient of Aqua results in greater vertical wind shear, stronger westward flows accumulating upward over the equator, and stronger subtropical and polar jets in the upper levels (Fig. 7a–b).

For the ocean, the defining horizontal circulations – zonal for Aqua and gyral for Ridge – are shown in Fig. 6c–d. On zonally unbounded Aqua, the rapid zonal flows result in  $\sim 1800$  Sv of globally integrated net zonal transport. On bounded Ridge, the gyral flows  $\sim O(100)$  Sv arise from Sverdrup dynamics, corresponding to the meridional distribution of surface wind stress (Fig. 4e–f). These gyres suggest analogues of the Pacific’s equatorial counter-currents and the western and eastern boundary systems. Fig. 7c–d presents the zonally averaged vertical structure of these currents in the zonal direction. On Aqua (Fig. 7c), the direction of the zonal currents corresponds to the surface wind stress (Fig. 4c), with velocity dampening towards zero deeper down. Near the surface, the maximum velocity of the westward current reaches  $2.29 \text{ ms}^{-1}$ . Ridge, in contrast, shows richer structure particularly in the tropics, with the presence of equatorial under- and counter-currents (Fig. 7d). The depth of the equatorial undercurrent at  $\sim 200$  m is consistent with the depth of the equatorial thermocline (Fig. 2i). These features are absent on Aqua, which cannot maintain zonal pressure gradients in its interior. Ridge’s maximum velocity, in the near-surface equatorial westward current, is  $0.44 \text{ m s}^{-1}$ , about an order of magnitude lower than Aqua’s. The effect of Ridge’s meridional boundary is also seen in the meridional overturning circulation of both the atmosphere and the ocean

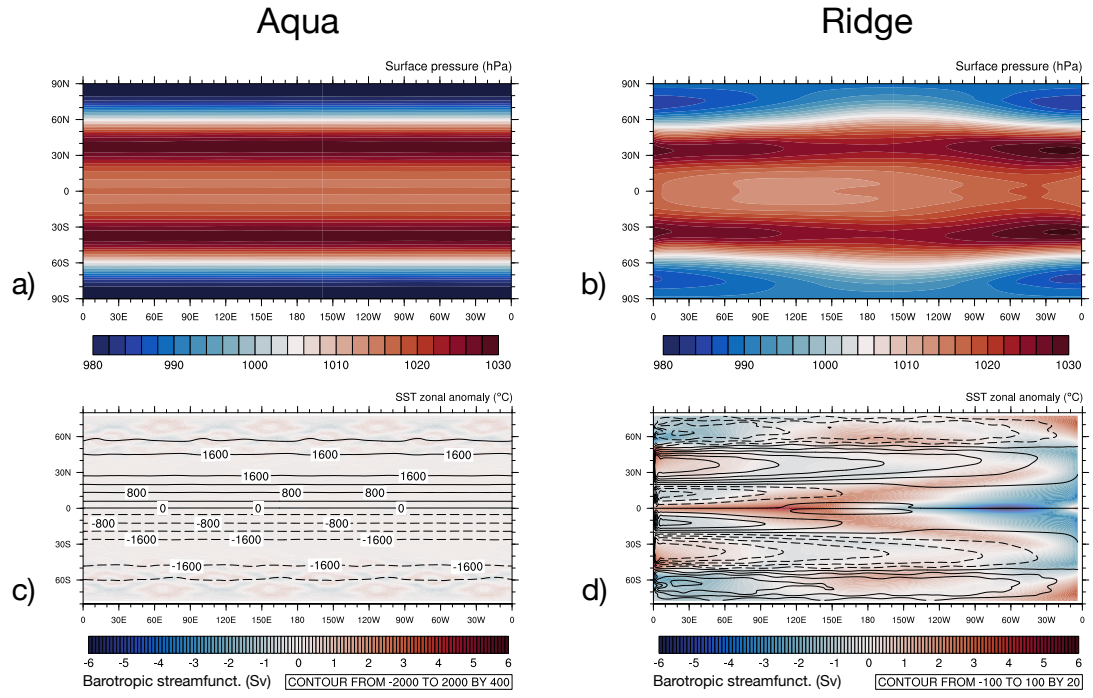


**Figure 6.** Plan views of 100-yr climatology: (a–b) Atmosphere: surface pressure (hPa); (c–d) Ocean: barotropic streamfunction (Sv, contour lines; solid is positive/clockwise, dashed is negative/counterclockwise), overlaid on the zonal anomaly of SST (°C, color shading). Note the difference in contouring intervals for the streamfunction (c–d). The pattern of Aqua’s SST zonal anomaly (panel c), barely visible, reflects the imprints of bottom topography.



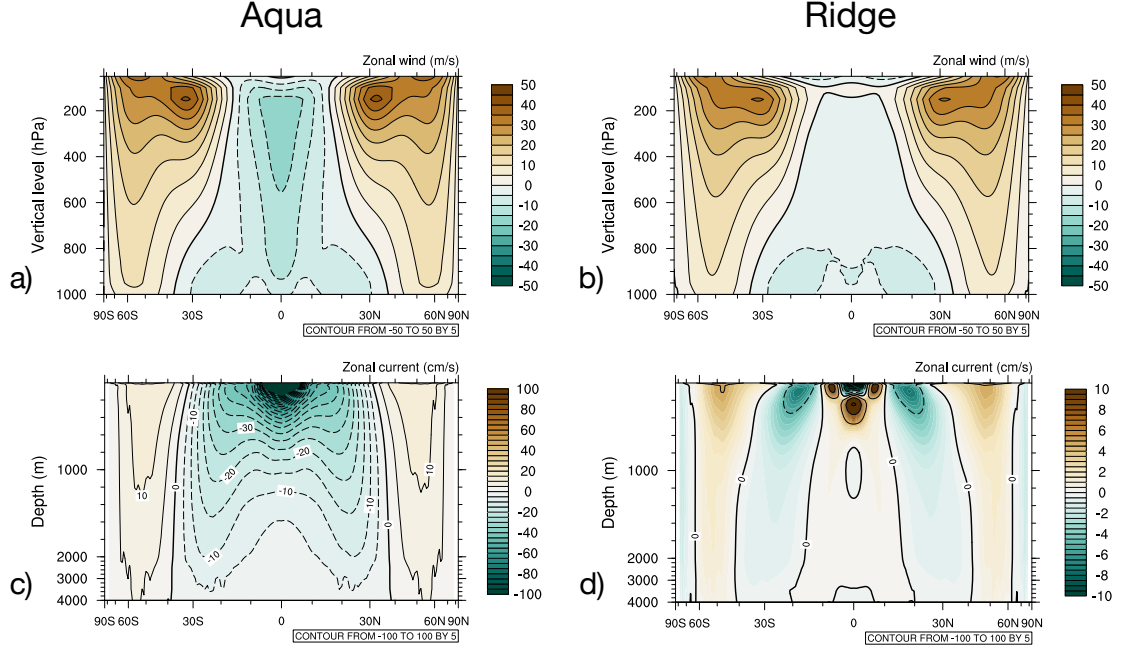


**Figure 7.** Zonally averaged vertical sections, 100-yr climatology: (a–b) Atmosphere: zonal wind ( $\text{ms}^{-1}$ ); (c–d) Ocean: zonal current ( $\text{cms}^{-1}$ ). Note that the color scale of panel (c) is an order of magnitude greater than panel (d).

(Fig. 8). For the atmosphere, in addition to the more familiar-looking overturning cells, the equatorial cold belt on Aqua leads to the formation of “reverse Hadley” cells in the deep tropics. On Ridge, this pattern is largely suppressed due to the western warm pool (Fig. 2, right column) that reduces the meridional gradient around the equatorial SST minimum in the zonal average (Fig. 4a). For the ocean, Aqua’s residual overturning broadly follows the isopycnals (Marshall & Radko, 2003; Wolfe & Cessi, 2011), forming deep subtropical cells (Fig. 8c). Alternatively, the residual overturning can be interpreted as the combination of the Eulerian mean and eddy components (see Fig. S4), where the compensating effect between the two components at high latitudes is analogous to the vanishing Deacon cell in the Southern Ocean (cf. Smith et al., 2006; Marshall et al., 2007). For Ridge, the presence of zonal pressure gradient largely reduces the depth of the subtropical overturning cells. Under the influence of polar convection, the mid-depth ( $\sim 1000$  m), diapycnal overturning cells in the midlatitudes are maintained by the balance between cooling via upwelling and diffusive heating (W. H. Munk, 1966; W. Munk & Wunsch, 1998).

An intriguing consequence of the “reverse Hadley” cells is observed in the seasonality of the ITCZs. The effect is most clearly seen in boreal or austral summer. Using boreal summer (June, July, and August) as an example, Fig. 9 shows the zonally averaged profiles of surface temperature and precipitation, and Fig. 10 shows the corresponding meridional overturning circulation in the atmosphere. For Aqua, despite higher SST in the summer hemisphere (Fig. 9a), its peak precipitation is in the winter hemisphere (Fig. 9b). This is a consequence of the persistence of Aqua’s equatorial cold belt throughout the seasonal cycle, which creates a stand-alone “reverse Hadley” cell in the winter hemisphere (Fig. 10a) over the local SST minimum (Fig. 9a). The ascending branch of this overturning cell, at  $\sim 10^\circ$  in the winter hemisphere, creates a narrow but extreme



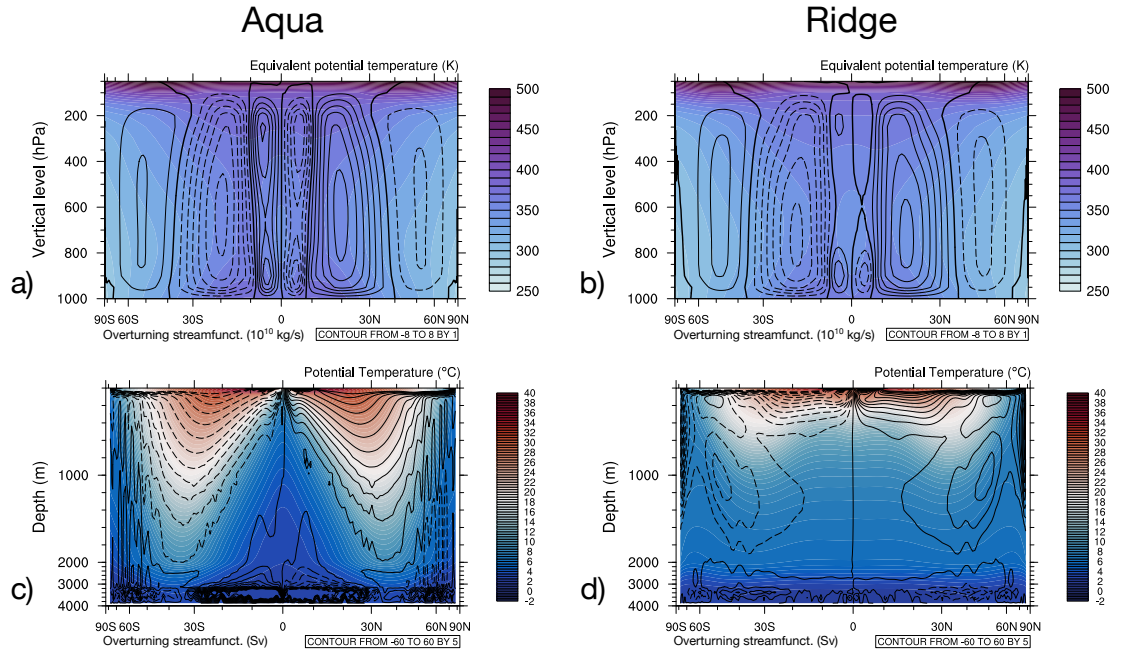


**Figure 8.** Zonally averaged vertical sections, 100-yr climatology: (a–b) Atmosphere: Eulerian meridional overturning streamfunction ( $10^{10} \text{ kg s}^{-1}$ , contour lines; solid is positive/clockwise, dashed is negative/counter-clockwise), overlaid on equivalent potential temperature (K, colored shading); (c–d) Ocean: residual overturning streamfunction (Sv, contour lines; solid is positive/clockwise, dashed is negative/counter-clockwise), overlaid on potential temperature ( $^{\circ}\text{C}$ , colored shading).

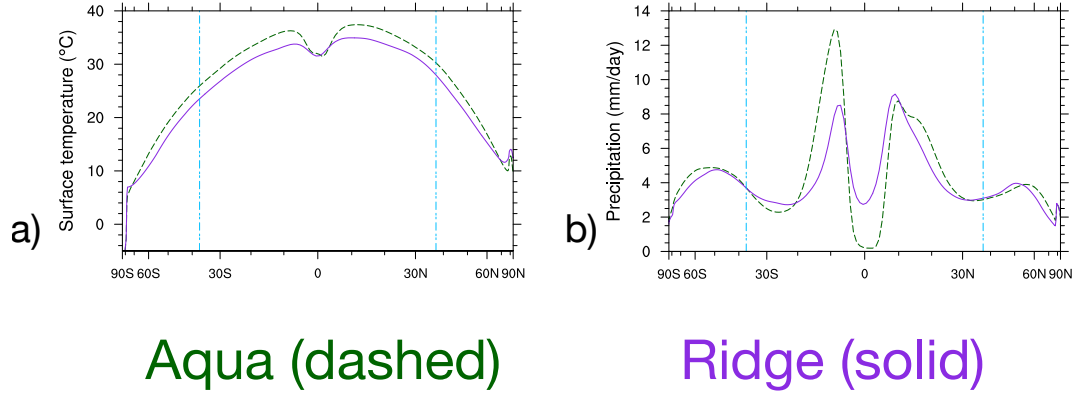


**Figure 9.** As Fig. 4(a–b), but for boreal summer (June, July, and August)

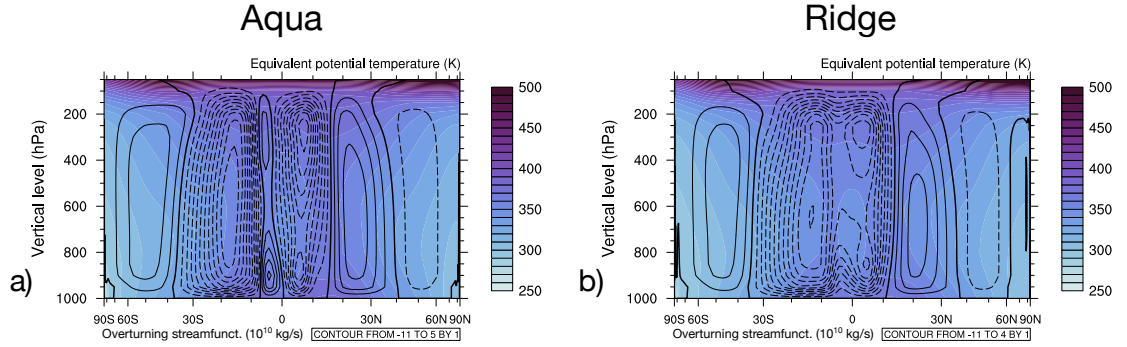


**Figure 10.** As Fig. 8(a–b), but for boreal summer (June, July, and August)

band of maximum precipitation (Fig. 9b) exceeding that of the summer hemisphere. In this regard, Ridge behaves more Earth-like: in the winter or summer season, although the presence of the eastern cold tongue manifests itself by affecting the magnitude of the cross-equatorial Hadley-like overturning (Fig. 10b), dynamically its convection-inducing effects in the winter flank are much reduced compared to Aqua’s case. For this reason, the zonally averaged maximum precipitation of Ridge remains in the summer hemisphere (Fig. 9b). As suggested by the somewhat counter-intuitive seasonal distribution of Aqua’s atmospheric moisture in Fig. 1c, this is yet another subtle aspect of how ocean geometry governs the state of the coupled climate, including the interaction between the large-scale circulation and the water cycle.

### 3.3 Meridional Heat Transport

The energy budget and circulation patterns of the two planets, as described by the previous subsections, drive the meridional heat transport (Fig. 11). For both planets, the total meridional heat transport peaks close to 6 PW in each hemisphere, at the bounds of the tropics. Ocean heat transport, dominating in the deep tropics, peaks at close to 4 PW for Aqua, and around 2 PW for Ridge. Atmospheric heat transport, dominating

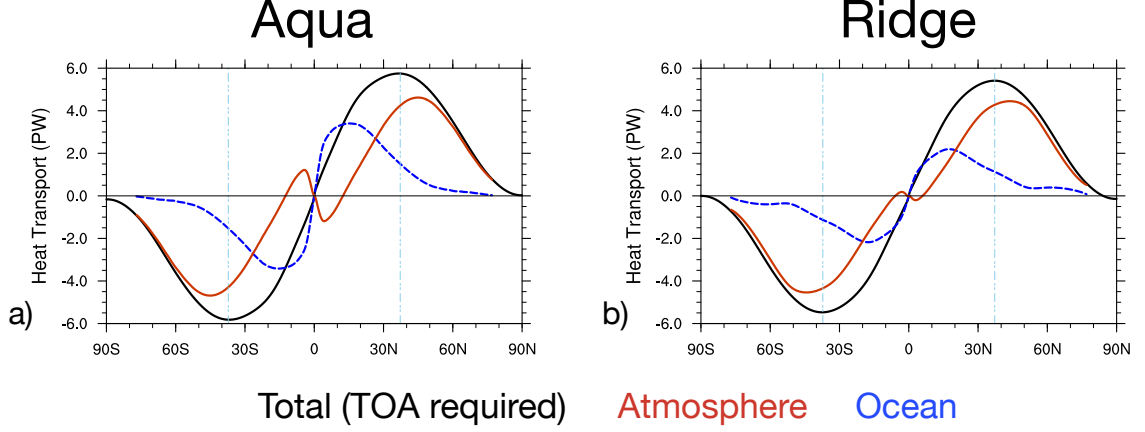


**Figure 11.** Meridional heat transport, 100-yr climatology: (a) Aqua; (b) Ridge. The vertical blue lines mark the extent of the tropics, as in Fig. 3(a–d) and Fig. 4.

in the extratropics, peaks around 50°N/S for both planets. Overall, as discussed by Enderton and Marshall (2009), the qualitative features and partition between the atmosphere and the ocean resemble Earth observations (Fasullo & Trenberth, 2008), with Ridge showing greater degrees of realism. Here we discuss the differences between Aqua and Ridge from energetic and dynamic perspectives (Armour et al., 2019).

Energetically, the TOA tropical surplus (Fig. 3c–d) requires greater amounts of total meridional heat transport for Aqua than Ridge. Likewise, the excessive net heating of Aqua’s tropical ocean (Fig. 3e) results in greater amounts of ocean heat transport out of the tropics than Ridge (Fig. 3f). In particular, over the equatorial region, since the net heating at ocean surface exceeds that of TOA, it is implied that the atmosphere must compensate by transporting energy equatorward for those regions (Fig. 11).

Dynamically, these requirements are fulfilled by the meridional overturning circulation in both fluids (Fig. 8). As detailed in Czaja and Marshall (2006), the meridional heat transport by either fluid can be viewed as decomposed into two factors: the magnitude of the meridional overturning, and the energy contrast between the poleward and equatorward branches, as measured by moist static energy for the atmosphere and potential temperature for the ocean. For the atmosphere, the equatorward heat transport over 10°N/S is delivered by the “reverse Hadley” cells (Fig. 8a–b), which transport higher amounts of moist static energy in their equatorward upper branches than their poleward lower branches, at greater magnitude of overturning on Aqua than Ridge. It is worth noting that the Eulerian mean overturning in Fig. 8a–b only reflects the atmospheric heat transport by the mean flow, which dominates in the tropics, but gives way to the eddy component at higher latitudes (cf. Enderton & Marshall, 2009). For the ocean, the energetically required ocean heat transport is accomplished by the residual overturning (Fig. 8c–d), where the thermal contrast between the poleward upper branch and equatorward lower branch is greater on Aqua than Ridge, as the equatorward branch of Aqua’s residual overturning reaches near the bottom. On Ridge (Fig. 11b), the “kinks” in ocean heat transport, or local maximum at ~20°N/S and local minimum at ~50°N/S, reflect the boundary of the gyres (Fig. 6d), absent on Aqua.

Overall, this comparison highlights the influence of the meridional boundary on meridional heat transport and its partition, via both the energetic requirements and the dynamics (Czaja & Marshall, 2006; Enderton & Marshall, 2009). Particularly, in light of

having better resolved “reverse Hadley” circulation than earlier investigations (Czaja & Marshall, 2006; Smith et al., 2006; Farneti & Vallis, 2009) and the corresponding equatorward heat transport by the atmosphere, we note the role of Ridge’s meridional boundary in shaping a more Earth-like pattern of meridional heat transport.

## 4 Conclusions and Discussion

In this study, we introduce the first two examples of fully coupled, idealized models developed in the CESM Simpler Models framework. Building upon previous idealized studies using aquaplanets at various degrees of complexity and atmosphere-ocean coupling, our work explores the coupled climate controlled by ocean geometry, represented by a meridional boundary present on Ridge and absent on Aqua. By using contemporary atmospheric and ocean model components at resolutions comparable to comprehensive Earth System Models, we aim to apply these idealized models to future studies of various features in the coupled climate system.

Contrasting the mean climates of the CESM Aqua and Ridge planets, the main conclusions are summarized as follows:

1. With sufficient horizontal and vertical resolution, Aqua manifests a global cold belt of equatorial upwelling, while Ridge develops zonal contrast between its western warm pool and eastern cold tongue due to boundary dynamics;
2. Energetically, Aqua’s cold belt results in a climate state  $\sim 2^\circ\text{C}$  warmer than Ridge on global average, due to the effects of tropical clouds and water vapor;
3. Dynamically, the meridional boundary of Ridge — with the resulting zonal asymmetry — is crucial for producing a climate system with more Earth-like features compared to Aqua, including atmospheric and ocean circulation, the seasonality of ITCZ, and the meridional heat transport.

In general, the CESM Aqua and Ridge planets present a number of qualitative features similar to those discussed by previous works (Smith et al., 2006; Enderton & Marshall, 2009; Farneti & Vallis, 2009), including the large-scale circulation and meridional heat transport. We discuss the following aspects of distinction from previous models:

1. **The climate contrast between Aqua and Ridge and the role of ocean geometry in planetary albedo.** Contrary to Enderton and Marshall (2009) where Aqua — with its sea ice — has a colder climate than the ice-free Ridge, in the present study ice-free CESM Aqua is warmer than Ridge. As discussed in Section 3.1, this is attributed to the tropical distribution of clouds, which largely dominates the planetary albedo in the absence of ice. Compared to ice-present climate states of Enderton and Marshall (2009), the contrast between ice-free Aqua and Ridge suggests a fundamentally different role of the ocean’s meridional boundary on the global climate: instead of reducing planetary albedo by the melting of sea ice via the ocean’s western boundary dynamics, the strip continent in CESM Ridge enhances planetary albedo through tropical clouds, via the formation of the western warm pool and atmospheric convection over it. While the quantitative effect likely depends on configurations of the atmospheric model including resolution, parameterization and other aspects affecting the representation of clouds (e.g. apparently minimized contrast in Smith et al., 2006), the qualitative contrast with Aqua has implications for the investigation of ice-free warm states in Earth’s history or future. From a practical standpoint, for alternative applications of the current CESM Aqua and Ridge models, colder climate states with sea ice — when desired for certain investigations — can potentially be achieved by parameter tuning in the atmospheric component.

2. **Aqua’s equatorial cold belt and the resulting “reverse Hadley” circulation.** In CESM Aqua, the atmospheric “reverse Hadley” cells over the equatorial belt of upwelling are more distinctively represented than earlier models (Smith et al., 2006; Marshall et al., 2007; Farneti & Vallis, 2009), providing stronger contrast against the corresponding Ridge configuration. While the coupled tropical dynamics of wind-driven equatorial upwelling and the corresponding atmospheric “reverse Hadley” cells are relatively straightforward, the representation of these features largely depends on the horizontal resolution of both model components for resolving the oceanic belt of upwelling and the narrow (less than  $10^\circ$  in the meridional extent) atmospheric cells. By using model components and resolution comparable to that of CMIP, the assessment of these features — in contrast to Ridge or additional forms of ocean geometry — will have direct relevance to eastern Pacific upwelling and the corresponding regional meridional cells (e.g. Sun et al., 2019) in realistic, coupled Earth configurations.
3. **The location and intensity of Ridge’s western warm pool, and the associated Walker circulation.** Compared to earlier Ridge models with a warm pool closer to the western boundary and a relatively weak zonal SST gradient (Smith et al., 2006; Enderton & Marshall, 2009; Farneti & Vallis, 2009), CESM Ridge has a climatological warm pool farther east (distance from the western boundary  $\sim 1/3$  of the basin width), and a zonal SST gradient comparable to the Pacific. Besides ocean dynamics, the roles of cloud forcing and wind stress in the formation of the warm pool are broadly consistent with some of earlier idealized studies on the Western Pacific (Clement et al., 2005; Watanabe, 2008a, 2008b). The question of controlling factors and mechanisms for the location and intensity of the warm pool can be a topic of further investigation in this coupled, idealized framework.

Furthermore, preliminary analysis on the sub-seasonal to interannual variability of Aqua and Ridge reveals promising features, including MJO- and ENSO-like modes on Ridge. These modes of tropical variability, in different forms for Aqua and Ridge with relevance to the interpretation of realistic Earth configurations, will be addressed in future work.

To conclude, the climate states of CESM Aqua and Ridge configurations showcase the capacity of the idealized coupled models to represent relatively well-understood dynamics, while further enabling more detailed investigation of the coupled climate system. The newly available capacities — including aspects of cloud radiative effects, convection, and circulation — are due to increased resolution and more complete physics of CMIP-class components. By using CESM components, the close relationship between these idealized configurations and comprehensive, realistic Earth configurations fills a long-standing gap in the idealized modeling hierarchy. This addition to the hierarchy opens up new potential for the investigation of coupled atmosphere-ocean processes, as well as serving as test beds for model evaluation and development. The Aqua and Ridge configurations presented here are expected to be available in the next major release of CESM as part of the Simpler Models suite, potentially with the software for creating additional, customized ocean geometries. Building on the two baseline configurations of Aqua and Ridge, increasingly complex ocean geometries may be explored (e.g. Ferreira et al., 2010). Furthermore, with increased atmospheric and/or ocean resolution, the CESM idealized coupled models can provide insights into an even wider range of features and scale interactions of scientific and societal interests in the coupled climate system.

## Acknowledgments

The simulation outputs under analysis are available on CISL’s Globally Accessible Data Environment. We thank the following collaborators for their help with simplified climate models (in alphabetical order): Alper Altuntas, Kyle Armour, David Bailey, Jim Benedict, Pedro Di Nezio, Erik Kluzek, Keith Lindsay, Brian Medeiros, Sarah Ragen, Mathew

Rothstein, and Andrew Shao. We also thank Anna-Lena Deppenmeier for helpful discussion on the manuscript. Wu was supported by National Science Foundation (NSF) grant AGS1648629, the Advanced Study Program of NCAR, and the Junior Researcher Award of the Institute for Advanced Computational Science at Stony Brook University. Reed was supported by NSF grants AGS1648629 and AGS1830729. The National Center for Atmospheric Research (NCAR) is sponsored by the NSF under Cooperative Agreement 1852977. We acknowledge computing and data storage resources, including the Cheyenne supercomputer (doi:10.5065/D6RX99HX), provided by the Computational and Information Systems Laboratory (CISL) at NCAR.

## References

- Abernathy, R., Ferreira, D., & Klocker, A. (2013). Diagnostics of isopycnal mixing in a circumpolar channel. *Ocean Modelling*, 72, 1–16.
- Adcroft, A., Anderson, W., Balaji, V., Blanton, C., Bushuk, M., Dufour, C. O., . . . others (2019). The GFDL global ocean and sea ice model OM4. 0: Model description and simulation features. *Journal of Advances in Modeling Earth Systems*, 11(10), 3167–3211.
- Armour, K. C., Siler, N., Donohoe, A., & Roe, G. H. (2019). Meridional atmospheric heat transport constrained by energetics and mediated by large-scale diffusion. *Journal of Climate*, 32(12), 3655–3680.
- Bachman, S., & Fox-Kemper, B. (2013). Eddy parameterization challenge suite I: Eady spindown. *Ocean Modelling*, 64, 12–28.
- Bailey, D., DuVivier, A., Holland, M., Hunke, E., Lipscomb, B., Briegleb, B., . . . Schramm, J. (2018). *CESM CICE5 users guide* (Tech. Rep.). Tech. rep.
- Ballinger, A. P., Merlis, T. M., Held, I. M., & Zhao, M. (2015). The sensitivity of tropical cyclone activity to off-equatorial thermal forcing in aquaplanet simulations [Journal Article]. *Journal of the Atmospheric Sciences*, 72(6), 2286–2302.
- Benedict, J. J., Medeiros, B., Clement, A. C., & Pendergrass, A. G. (2017). Sensitivities of the hydrologic cycle to model physics, grid resolution, and ocean type in the aquaplanet Community Atmosphere Model. *Journal of Advances in Modeling Earth Systems*, 9(2), 1307–1324.
- Blackburn, M., Williamson, D. L., Nakajima, K., Ohfuchi, W., Takahashi, Y. O., Hayashi, Y.-Y., . . . others (2013). The aqua-planet experiment (APE): Control SST simulation. *Journal of the Meteorological Society of Japan. Ser. II*, 91, 17–56.
- Bleck, R. (1978). On the use of hybrid vertical coordinates in numerical weather prediction models. *Monthly weather review*, 106(9), 1233–1244.
- Brunetti, M., Kasparian, J., & V  rard, C. (2019). Co-existing climate attractors in a coupled aquaplanet. *Climate Dynamics*, 53(9-10), 6293–6308.
- Carranza, M. M., Gille, S. T., Franks, P. J., Johnson, K. S., Pinkel, R., & Garton, J. B. (2018). When mixed layers are not mixed: Storm-driven mixing and bio-optical vertical gradients in mixed layers of the southern ocean. *Journal of Geophysical Research: Oceans*, 123(10), 7264–7289.
- Cessi, P., & Jones, C. S. (2017). Warm-route versus cold-route interbasin exchange in the meridional overturning circulation. *J. Phys. Oceanogr.*, 47(8), 1981–1997.
- Chang, K.-I., Ghil, M., Ide, K., & Lai, C.-C. A. (2001). Transition to aperiodic variability in a wind-driven double-gyre circulation model. *Journal of physical oceanography*, 31(5), 1260–1286.
- Chavas, D. R., Reed, K. A., & Knaff, J. A. (2017). Physical understanding of the tropical cyclone wind-pressure relationship [Journal Article]. *Nature communications*, 8(1), 1360.



- Clement, A. C., Seager, R., & Murtugudde, R. (2005). Why are there tropical warm pools? *Journal of climate*, 18(24), 5294–5311.
- Collins, M., Knutti, R., Arblaster, J., Dufresne, J.-L., Fichefet, T., Friedlingstein, P., ... others (2013). Long-term climate change: projections, commitments and irreversibility. In *Climate change 2013-the physical science basis: Contribution of working group I to the fifth assessment report of the intergovernmental panel on climate change* (pp. 1029–1136). Cambridge University Press.
- Czaja, A., & Marshall, J. (2006). The partitioning of poleward heat transport between the atmosphere and ocean [Journal Article]. *Journal of the atmospheric sciences*, 63(5), 1498–1511.
- Danabasoglu, G., Lamarque, J.-F., Bacmeister, J., Bailey, D., DuVivier, A., Edwards, J., ... others (2020). The Community Earth System Model version 2 (CESM2). *Journal of Advances in Modeling Earth Systems*, 12(2), e2019MS001916.
- Donohoe, A., Frierson, D. M., & Battisti, D. S. (2014). The effect of ocean mixed layer depth on climate in slab ocean aquaplanet experiments [Journal Article]. *Climate dynamics*, 43(3-4), 1041–1055.
- Enderton, D., & Marshall, J. (2009). Explorations of atmosphere–ocean–ice climates on an aquaplanet and their meridional energy transports. *Journal of the Atmospheric Sciences*, 66(6), 1593–1611.
- Eyring, V., Bony, S., Meehl, G. A., Senior, C. A., Stevens, B., Stouffer, R. J., & Taylor, K. E. (2016). Overview of the Coupled Model Intercomparison Project Phase 6 (CMIP6) experimental design and organization. *Geoscientific Model Development (Online)*, 9(LLNL-JRNL-736881).
- Farneti, R., & Vallis, G. (2009). An Intermediate Complexity Climate Model (IC-CMp1) based on the GFDL flexible modelling system. *Geoscientific Model Development*, 2(2), 73.
- Fasullo, J. T., & Trenberth, K. E. (2008). The annual cycle of the energy budget. part II: Meridional structures and poleward transports. *Journal of Climate*, 21(10), 2313–2325.
- Ferrari, R., Nadeau, L.-P., Marshall, D. P., Allison, L. C., & Johnson, H. L. (2017). A model of the ocean overturning circulation with two closed basins and a reentrant channel. *J. Phys. Oceanogr.*, 47(12), 2887–2906.
- Ferreira, D., Marshall, J., & Campin, J.-M. (2010). Localization of deep water formation: Role of atmospheric moisture transport and geometrical constraints on ocean circulation [Journal Article]. *Journal of Climate*, 23(6), 1456–1476.
- Frierson, D. M., Hwang, Y.-T., Fučkar, N. S., Seager, R., Kang, S. M., Donohoe, A., ... Battisti, D. S. (2013). Contribution of ocean overturning circulation to tropical rainfall peak in the northern hemisphere [Journal Article]. *Nature Geoscience*, 6(11), 940–944.
- Gent, P. R., Willebrand, J., McDougall, T. J., & McWilliams, J. C. (1995). Parameterizing eddy-induced tracer transports in ocean circulation models. *Journal of Physical Oceanography*, 25(4), 463–474.
- Griffies, S. M., Levy, M., Adcroft, A. J., Danabasoglu, G., Hallberg, R. W., Jacobson, D., ... Ringler, T. (2015). Theory and numerics of the Community Ocean Vertical Mixing (CVMIX) project. *Tech. Rep.*.
- Grist, J. P., & Josey, S. A. (2003). Inverse analysis adjustment of the SOC air–sea flux climatology using ocean heat transport constraints. *Journal of Climate*, 16(20), 3274–3295.
- Hack, J. J. (1994). Parameterization of moist convection in the National Center for Atmospheric Research community climate model (CCM2). *Journal of Geophysical Research: Atmospheres*, 99(D3), 5551–5568.
- Held, I. M. (2005). The gap between simulation and understanding in climate modeling. *Bulletin of the American Meteorological Society*, 86(11), 1609–1614.
- Herrington, A. R., & Reed, K. A. (2017). An explanation for the sensitivity of the



- mean state of the community atmosphere model to horizontal resolution on aquaplanets. *Journal of Climate*, 30(13), 4781–4797.
- Hirt, C. W., Amsden, A. A., & Cook, J. (1974). An arbitrary Lagrangian-Eulerian computing method for all flow speeds. *Journal of computational physics*, 14(3), 227–253.
- Holloway, G. (1997). Eddy transport of thickness and momentum in layer and level models. *Journal of physical oceanography*, 27(6), 1153–1157.
- Holtstlag, A., & Boville, B. (1993). Local versus nonlocal boundary-layer diffusion in a global climate model. *Journal of Climate*, 6(10), 1825–1842.
- Hurrell, J. W., Holland, M. M., Gent, P. R., Ghan, S., Kay, J. E., Kushner, P. J., ... others (2013). The Community Earth System Model: a framework for collaborative research. *Bulletin of the American Meteorological Society*, 94(9), 1339–1360.
- Jeevanjee, N., Hassanzadeh, P., Hill, S., & Sheshadri, A. (2017). A perspective on climate model hierarchies. *Journal of Advances in Modeling Earth Systems*, 9(4), 1760–1771.
- Jones, C. S., & Cessi, P. (2016). Interbasin transport of the meridional overturning circulation. *J. Phys. Oceanogr.*, 46(4), 1157–1169.
- Jones, C. S., & Cessi, P. (2017). Size matters: Another reason why the Atlantic is saltier than the Pacific. *J. Phys. Oceanogr.*, 47(11), 2843–2859.
- Jones, C. S., & Cessi, P. (2018). Components of upper-ocean salt transport by the gyres and the meridional overturning circulation. *J. Phys. Oceanogr.*, 48(10), 2445–2456.
- Kaspi, Y., & Schneider, T. (2011). Downstream self-destruction of storm tracks [Journal Article]. *Journal of the Atmospheric Sciences*, 68(10), 2459–2464.
- Kessler, W. S. (2006). The circulation of the eastern tropical Pacific: A review. *Progress in Oceanography*, 69(2-4), 181–217.
- Large, W. G., McWilliams, J. C., & Doney, S. C. (1994). Oceanic vertical mixing: A review and a model with a nonlocal boundary layer parameterization. *Reviews of Geophysics*, 32(4), 363–403.
- Lawrence, D. M., Fisher, R. A., Koven, C. D., Oleson, K. W., Swenson, S. C., Bonan, G., ... others (2019). The community land model version 5: Description of new features, benchmarking, and impact of forcing uncertainty. *Journal of Advances in Modeling Earth Systems*.
- Li, H., & Sriver, R. L. (2018). Impact of tropical cyclones on the global ocean: Results from multi-decadal global ocean simulations isolating tropical cyclone forcing [Journal Article]. *Journal of Climate*(2018).
- Lin, S.-J., & Rood, R. B. (1996). Multidimensional flux-form semi-Lagrangian transport schemes. *Monthly Weather Review*, 124(9), 2046–2070.
- Lin, S.-J., & Rood, R. B. (1997). An explicit flux-form semi-Lagrangian shallow-water model on the sphere. *Quarterly Journal of the Royal Meteorological Society*, 123(544), 2477–2498.
- Maher, P., Gerber, E. P., Medeiros, B., Merlis, T. M., Sherwood, S., Sheshadri, A., ... Zurita-Gotor, P. (2019). Model hierarchies for understanding atmospheric circulation. *Reviews of Geophysics*, 57(2), 250–280.
- Manabe, S., & Bryan, K. (1969). Climate calculations with a combined ocean-atmosphere model. *Journal of the Atmospheric Sciences*, 26(4), 786–789.
- Marshall, J., Ferreira, D., Campin, J.-M., & Enderton, D. (2007). Mean climate and variability of the atmosphere and ocean on an aquaplanet [Journal Article]. *Journal of the Atmospheric Sciences*, 64(12), 4270–4286.
- Marshall, J., & Radko, T. (2003). Residual-mean solutions for the antarctic circumpolar current and its associated overturning circulation. *Journal of Physical Oceanography*, 33(11), 2341–2354.
- Medeiros, B., Williamson, D. L., & Olson, J. G. (2016). Reference aquaplanet climate in the Community Atmosphere Model, Version 5. *Journal of Advances in*

- 671 *Modeling Earth Systems*, 8(1), 406–424.
- 672 Molteni, F. (2003). Atmospheric simulations using a GCM with simplified phys-  
673 ical parametrizations. I: Model climatology and variability in multi-decadal  
674 experiments. *Climate Dynamics*, 20(2-3), 175–191.
- 675 Munk, W., & Wunsch, C. (1998). Abyssal recipes II: Energetics of tidal and wind  
676 mixing. *Deep-sea research. Part I, Oceanographic research papers*, 45(12),  
677 1977–2010.
- 678 Munk, W. H. (1966). Abyssal recipes. *Deep Sea Research and Oceanographic Ab-*  
679 *stracts*, 13(4), 707–730.
- 680 Neale, R. B., Chen, C.-C., Gettelman, A., Lauritzen, P. H., Park, S., Williamson,  
681 D. L., ... others (2010). Description of the NCAR Community Atmosphere  
682 Model (CAM 4.0). *NCAR Tech. Note NCAR/TN-486+ STR*, 1(1), 1–12.
- 683 Neale, R. B., & Hoskins, B. J. (2000). A standard test for AGCMs including their  
684 physical parametrizations: I: The proposal. *Atmospheric Science Letters*, 1(2),  
685 101–107.
- 686 Nilsson, J., Langen, P. L., Ferreira, D., & Marshall, J. (2013). Ocean basin geometry  
687 and the salinification of the atlantic ocean. *Journal of Climate*, 26(16), 6163–  
688 6184.
- 689 Pendergrass, A. G., & Hartmann, D. L. (2014). The atmospheric energy constraint  
690 on global-mean precipitation change. *Journal of climate*, 27(2), 757–768.
- 691 Polvani, L., Clement, A., Medeiros, B., Benedict, J., & Simpson, I. (2017). When  
692 less is more: Opening the door to simpler climate models, Eos, 98. *Eos, Trans-*  
693 *actions American Geophysical Union*, 99(3), 15–16.
- 694 Redi, M. H. (1982). Oceanic isopycnal mixing by coordinate rotation. *Journal of*  
695 *Physical Oceanography*, 12(10), 1154–1158.
- 696 Reed, K. A., & Jablonowski, C. (2012). Idealized tropical cyclone simulations of in-  
697 termediate complexity: A test case for AGCMs. *Journal of Advances in Model-*  
698 *ing Earth Systems*, 4(2).
- 699 Schultz, D. M., Fairman Jr, J. G., Anderson, S., & Gardner, S. (2017). Build your  
700 own earth: A web-based tool for exploring climate model output in teaching  
701 and research. *Bulletin of the American Meteorological Society*, 98(8), 1617–  
702 1623.
- 703 Scoccimarro, E., Fogli, P. G., Reed, K. A., Gualdi, S., Masina, S., & Navarra, A.  
704 (2017). Tropical cyclone interaction with the ocean: The role of high-frequency  
705 (subdaily) coupled processes [Journal Article]. *Journal of Climate*, 30(1),  
706 145–162.
- 707 Smith, R. S., Dubois, C., & Marotzke, J. (2006). Global climate and ocean circula-  
708 tion on an aquaplanet ocean–atmosphere general circulation model. *Journal of*  
709 *climate*, 19(18), 4719–4737.
- 710 Solomon, H. (1971). On the representation of isentropic mixing in ocean circulation  
711 models. *Journal of Physical Oceanography*, 1(3), 233–234.
- 712 Stephens, G. L., O’Brien, D., Webster, P. J., Pilewski, P., Kato, S., & Li, J.-l.  
713 (2015). The albedo of earth. *Reviews of geophysics*, 53(1), 141–163.
- 714 Sun, Y., Li, L. Z., Ramstein, G., Zhou, T., Tan, N., Kageyama, M., & Wang, S.  
715 (2019). Regional meridional cells governing the interannual variability of the  
716 hadley circulation in boreal winter. *Climate dynamics*, 52(1-2), 831–853.
- 717 Vallis, G. K., & Farneti, R. (2009). Meridional energy transport in the coupled  
718 atmosphere–ocean system: Scaling and numerical experiments. *Quarterly Jour-*  
719 *nal of the Royal Meteorological Society: A journal of the atmospheric sciences,*  
720 *applied meteorology and physical oceanography*, 135(644), 1643–1660.
- 721 Voigt, A., & Shaw, T. A. (2015). Circulation response to warming shaped by radia-  
722 tive changes of clouds and water vapour. *Nature Geoscience*, 8(2), 102–106.
- 723 Watanabe, M. (2008a). Two regimes of the equatorial warm pool. part I: A simple  
724 tropical climate model. *Journal of climate*, 21(14), 3533–3544.

- 725 Watanabe, M. (2008b). Two regimes of the equatorial warm pool. part II: Hybrid  
726 coupled GCM experiments. *Journal of climate*, *21*(14), 3545–3560.
- 727 Wolfe, C. L., & Cessi, P. (2010). What sets the strength of the middepth stratifica-  
728 tion and overturning circulation in eddying ocean models? *Journal of Physical*  
729 *Oceanography*, *40*(7), 1520–1538.
- 730 Wolfe, C. L., & Cessi, P. (2011). The adiabatic pole-to-pole overturning circulation.  
731 *Journal of Physical Oceanography*, *41*(9), 1795–1810.
- 732 Wyrski, K. (1981). An estimate of equatorial upwelling in the pacific. *Journal of*  
733 *Physical Oceanography*, *11*(9), 1205–1214.
- 734 Zhang, G. J., & McFarlane, N. A. (1995). Sensitivity of climate simulations to  
735 the parameterization of cumulus convection in the Canadian Climate Centre  
736 general circulation model. *Atmosphere-ocean*, *33*(3), 407–446.